Spin splitting in n-type $Bi_{1-x}Sb_x$ alloys including doped bismuth ($0 \leq x \leq 0.12$)

H. Köhler, H. J. Leister, and A. Gensler
Physikalisches Institut, Universität Würzburg, 8700 Würzburg, Federal Republic of Germany
(Received 26 June 1989; revised manuscript received 3 October 1989)

The crystals were grown from perfectly alloyed ingots and subsequent twofold zone melting in the opposite direction. Variable electron concentrations in the triple L conduction band were adjusted by additional doping with tellurium, in such a way that charge transport results from the contribution by electrons exclusively. Quantum oscillations in the magnetoresistance are complex for arbitrary orientation in the magnetic field as a result of a superposition of contributions by three strongly anisotropic Fermi surfaces, but may be analyzed reliably for the magnetic field **B** parallel to the trigonal axis and almost parallel to the binary axes. It shows up that in some directions of **B** the spin splitting is essentially higher than the cyclotron energy, contrary to the expectation from the two-band model. An inclusion of $k_x^2 k_y^2$ and $k_y^2 k_z^2$ terms in the $E(1+E/E_g)$ dispersion appears to be necessary for a comprehensive interpretation.

I. INTRODUCTION

Quantum oscillations in the magnetoresistance were first detected on semimetallic bismuth in 1930.[1] Considerable experimental and theoretical work was dedicated to the investigation of the electronic properties of this crystal system and of Bi-Sb alloys in the almost six decades since. There were always some problems in growing homogeneous $Bi_{1-x}Sb_x$ single crystals as a result of segregation of the components during the growth process. This difficulty is overcome completely in our samples by a twofold, successive zone melting in the opposite direction after previous perfect alloying. This technique, in addition, allows a homogeneous chemical doping of the crystal bars, e.g., with tin (p type) or tellurium (n type). The latter was applied here for compositions $0 \leq x \leq 0.12$ in order to achieve exclusive charge transport by electrons with adjustable concentration N in the semiconducting and semimetallic crystals, i.e., for any composition and liquid-helium temperatures the chemical potential is adjusted above the T valence-band maximum. In our samples N was deduced to be between about 2×10^{17} and 4×10^{18} cm^{-3}. Of course, lower electron mobilities caused by doping must be set against the advantage of a single type of charge carrier; in general, however, the doping yields a benefit on balance for the interpretation of the experiments.

The constant-energy surfaces and $E(\mathbf{k})$ relations of the conduction and valence band around the triple L points of the Brillouin zone are discussed in ellipsoidal parabolic (EP), ellipsoidal nonparabolic (ENP, Lax[2]) nonellipsoidal nonparabolic (NENP, Cohen[3]) and modified nonellipsoidal nonparabolic (MNENP) (e.g., see McClure and Choi[4]) models, and for many purposes the ENP description primarily appeared to be sufficient (e.g., Cohen and Blount,[5] Smith *et al.*,[6] and McCombe *et al.*[7]). There are several modifications of the $E(\mathbf{k})$ relation, such as the "full" Cohen model,[3] the Abrikosov-Falkovsky model,[8] and the Baraff model[9] (including the effect of other bands), which were established as extensions of the simpler models in order to allow an optimum of interpretation of the experimental results. The work of Dresselhaus and co-workers[10,11] is cited here as examples of magneto-optical investigations in this field.

Considerable anisotropy of the $E(\mathbf{k})$ relation makes a decision between the ENP and NENP (including MNENP) cases difficult from an investigation of magnetoquantum oscillations, since absolute values of three different, superimposed Shubnikov–de Haas frequencies with, in general, deviating spin splitting and level broadening have to be discerned, which is difficult for arbitrary orientations in the magnetic field. The detailed, previous work on this subject will not be extended here. However, the spin splitting Δ_s—if resolved—only from a single-quantum oscillation may give evidence for a deviation from the value equal to the Landau splitting, expected from a two-band model. In particular, half-integer values for the ratio $M=\Delta_s/(\hbar\omega_c)=gm_c/(2m_0)$ should clearly be resolved in the oscillatory patterns. Although here also in the arbitrary case the superposition of the different oscillations may impede a clear decision, for $\mathbf{B}\|\mathbf{c}$ (single frequency) and for **B** almost parallel to a binary axis (separation of two oscillations in the magnetic field scale) a direct access to additional structure in the quantum oscillations from spin splitting is possible with high reliability. Such investigations are presented below.

II. EXPERIMENTAL RESULTS

The electron concentration N in the conduction band could be deduced from the saturation value of the Hall constant $R_{H\infty}=-(eN)^{-1}$ directly, since in any case a completely filled T valence band was realized by chemical doping. A typical magnetoquantum oscillation for $\mathbf{B}\|\mathbf{n}$ (**n** denotes one of the binary axes) in the longitudinal voltage U_{pp} between potential probes (measured parallel to the constant sample current) is shown in Fig. 1. The low-frequency (LF) oscillation below $B\approx3.5$ T originates from the two smaller, equivalent extremal cross-sectional

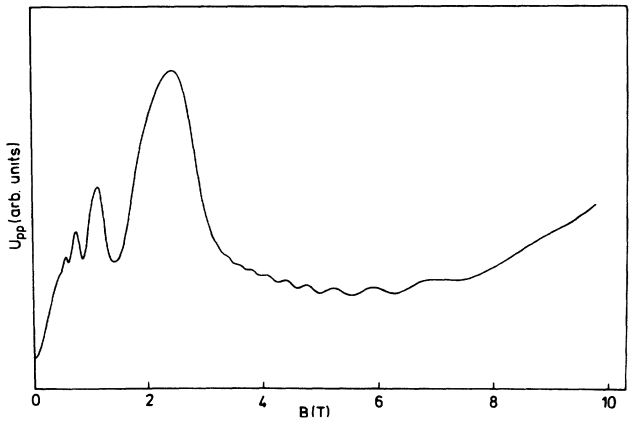

FIG. 1. Magnetoquantum oscillations in the resistance (proportional to the voltage U_{pp} between potential probes for constant current) of a $Bi_{1-x}Sb_x$ sample ($x=0.09$) with **B** aligned parallel to a binary axis (**n**) for $T=1.5$ K.

areas of the Fermi surfaces, the high-frequency (HF) oscillation above corresponds to the largest extremal cross-sectional area of the remaining third Fermi surface (L point of Brillouin zone). Towards high fields ($B \gtrsim 7$ T) the HF oscillatory amplitude dependence (despite exclusive electron conduction) is complicated by essential charge transfer between the different valleys (see the discussion below).

A phase analysis for each of the LF and HF extrema positions of Fig. 1 (U_{pp} maxima associated with integers n are plotted as a function of the appertaining B_{max}^{-1} values) is shown in Fig. 2. For the LF maxima it yields a straight-line dependence (constant-electron concentration in both valleys), which may be extrapolated towards $B_{max}^{-1}=0$. The almost-integer intersection with the ordinate axis is compatible with a finite (but unresolved) spin splitting for $M=gm_c/(2m_0)\approx 1,3,\ldots$, since in the maxima of $U_{pp}\sim\rho_{xx}\approx\sigma_{xx}/\sigma_{xy}^2$ (for transverse configuration, constant current, and $\sigma_{xy}^2 \gg \sigma_{xx}^2$) the respective Landau subbands with level broadening are half-filled approximately in the maxima of their density of states. It is reasonable to assume $M\approx 1$, in good agreement with the two-band model characteristics. The HF oscillation (Fig. 1) is observed in the quantum limit of the LF oscillation where the chemical potential of this subsystem should become field dependent, for increasing B aimed at a decrease towards the conduction-band edge for $M=1$. Since E_F(HF) alone for $B \lesssim 10$ T should be almost field independent outside its quantum limit, an electron charge transfer into the LF valleys occurs with increasing B. This is also demonstrated in Fig. 2, where n(HF) over the B_{max}^{-1} values for the HF oscillation yields a nonlinear dependence as a result of a shrinking extremal cross-sectional area of the Fermi surface with increasing B, i.e., with decreasing n(HF) (the slope in Fig. 2 is proportional to the extremal cross-sectional area decreasing with decreasing B^{-1}). From this reason, no reliable extrapolation towards $B_{max}^{-1}=0$ and no phase analysis is possible. The result also impedes a determination of the quantum numbers involved.

For **B**$\|$**s** (**s** denotes one of the bisectrix axes), two quantum oscillations are superimposed in the whole range of B with a 2:1 ratio of their frequencies. The phase analysis for both oscillations allows a linear extrapolation, the results in both cases also being compatible with $M\approx 1$, in agreement with the expectation from a two-band model ($M=1$).

The sample alignment for **B**$\|$**c** (**c** denotes the trigonal axis) is difficult (necessary to at least better than 0.5°), in this case yielding a single and regular magnetoquantum oscillation (Fig. 3) and the absence of electron transfer between the three equivalent valleys. In the second derivative $d^2U_{pp}/dB^2=U_{pp}''$ (not shown here) more structure is resolved in the maximum near $B=8$ T which cannot be removed by improved alignment. It indicates a small deviation from an integer value of M (about 0.2). A numerical simulation $\rho_{xx}(B)$ is also shown in Fig. 3 (to be discussed in Sec. III). The phase analysis (Fig. 4), outside the error margins, allows a linear extrapolation with an intersection of the ordinate axis at a half-integer value,

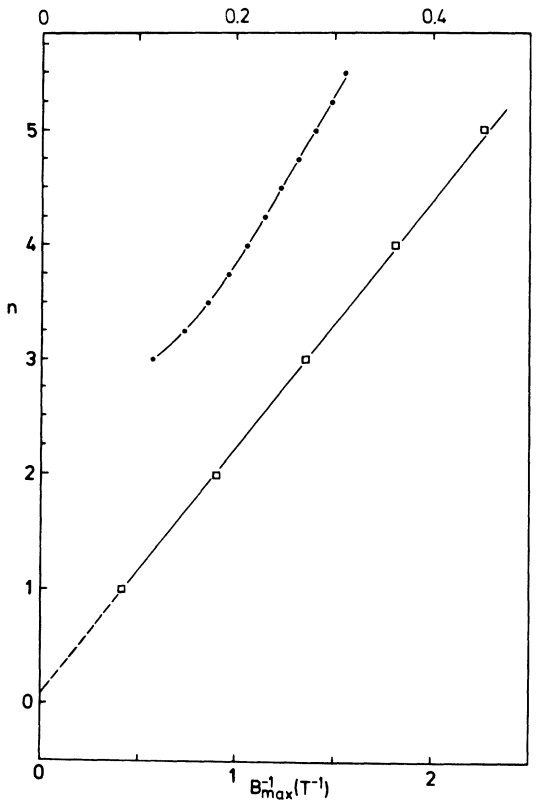

FIG. 2. Integers n for the U_{pp} maxima of the low- (LF) and high-frequency (HF) oscillation of Fig. 1 as a function of the pertinent B_{max}^{-1} values. The linear dependence (LF denoted by □) may be extrapolated (dashed line) towards $B^{-1}=0$, yielding an almost integer intersection. The HF data (●) with a spread-out B^{-1} scale (factor of 5; upper abscissa) and compressed ordinate graduation (factor 4) are influenced by electron transfer between the valley systems as a function of B, which impedes an extrapolation and phase analysis. For a discussion see the text.

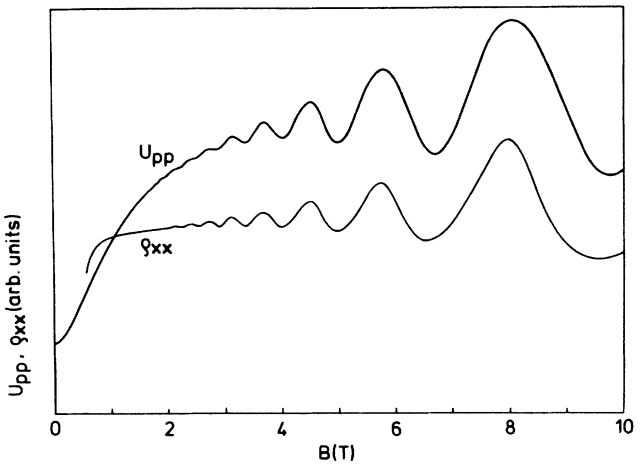

FIG. 3. Magnetoquantum oscillations in U_{pp} for a similar sample as Fig. 1 ($x=0.09$; same crystal bar) for $\mathbf{B}\|\mathbf{c}$ (c; trigonal axis) with an error of alignment less than 0.5°. The numerical simulation for $M=gm_c/(2m_0)=0$ is discussed in Sec. III.

clearly deviating from the expectation for a two-band model. The reduced quality of our doped samples in comparison with pure bismuth, nevertheless, allows an unequivocal statement from the phase analysis, which is prevented when T valence-band holes contribute to the conductivity essentially.

A reliable confirmation of this conclusion is obtained from samples with lower electron concentration, allowing us to reach the quantum limit.[12–14] The quantum oscillation for $\mathbf{B}\|\mathbf{c}$ of such a sample with low electron concentration is shown in Fig. 5 ($N=2.1\times10^{17}$ cm^{-3}) where, actually, the last U_{pp} maximum is reached near $B=9.5$ T [i.e., $E_F(B)$ roughly coincides with the maximum in the density of states of the $n=0\downarrow$ ($M\approx0$) or the $n=1\uparrow$ ($M\approx2$) Landau subband, corresponding to an approximate semioccupation of this system]. The phase analysis in Fig. 6 again confirms a half-integer intersection of the ordinate axis for a linear extrapolation, excluding the last U_{pp} minimum and maximum towards the quantum limit. For $M\approx0$ the last maximum should almost coincide with the dotted straight line; for $M\approx2$ the deviation is expected. The latter case is corroborated in Fig. 5 by the numerical calculation of $\rho_{xx}(B)$ and $E_F(B)$ with $M=2$ (see the discussion in Sec. III). Regardless, there is a finite spin splitting (confirmed by the unambiguous occurrence of the last maximum near $B=9.5$ T), which clearly deviates from $\hbar\omega_c$. This result, realized on several samples, is contrary to the two-band model assumed as a general basis for most of the directions of the energy dispersion of the L electrons so far.

In the best samples with somewhat higher electron concentrations, the effective spin splitting for $\mathbf{B}\|\mathbf{c}$ is resolved in U_{pp} by a weak high-field shoulder on the maximum near $B=8.5$ T in Fig. 7. The numerical simulation of the $n=0\downarrow$ peak in $\rho_{xx}(B)$ starts to become visible for $M=1.9$ with a reasonable level broadening (see the discussion in Sec. III).

Tilting the samples in the magnetic field perpendicular to the c axis, away from the binary axes by only a few degrees, the separation of the LF and HF oscillations in the

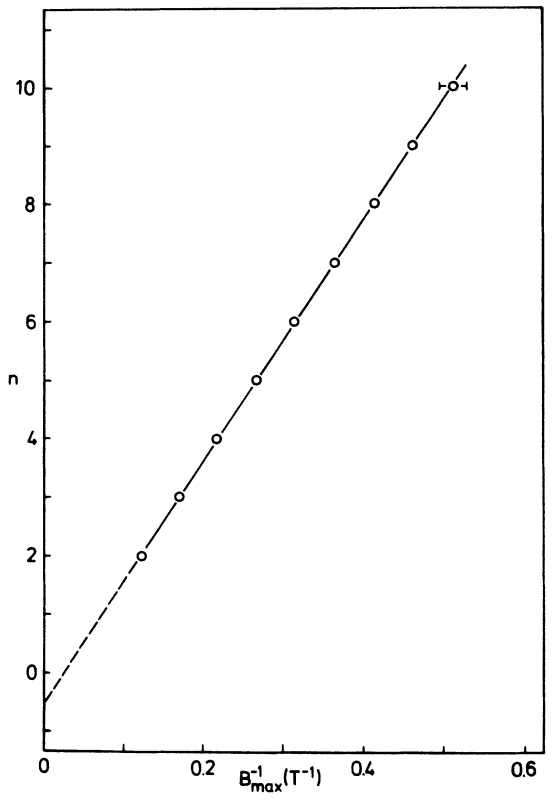

FIG. 4. $n=n(B_{max}^{-1})$ plot for the data of Fig. 3 ($\mathbf{B}\|\mathbf{c}$). The extrapolation (dashed line) of the linear dependence (solid line) yields a half-integer intersection at $B^{-1}=0$. The low-field error bar is indicated, and the high-field uncertainty is smaller than the symbol diameter.

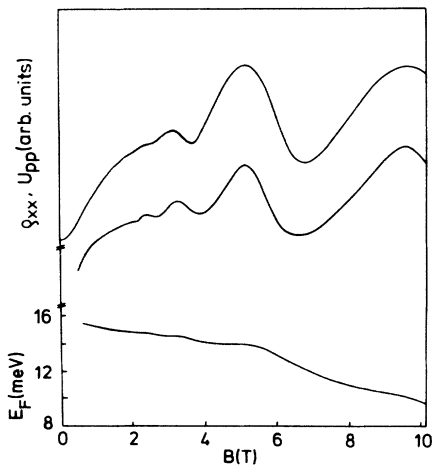

FIG. 5. Magnetoquantum oscillations in U_{pp} for $\mathbf{B}\|\mathbf{c}$ of a sample with $x=0.1$ and $N=2.1\times10^{17}$ cm^{-3} at $T=1.5$ K. The numerical simulation (ρ_{xx} and E_F) for $M=gm_c/(2m_0)=2$ is discussed in Sec. III.

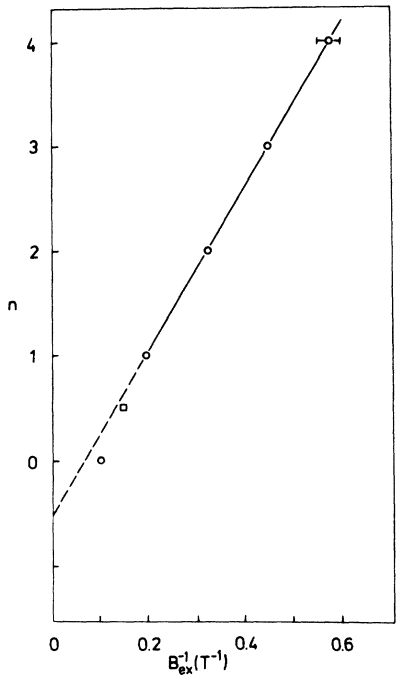

FIG. 6. $n=n(B_{ex}^{-1})$ plot for the results of Fig. 5 where the circles represent the maxima and the square represents the last U_{pp} minimum. The extrapolation (dashed line) yields a half-integer value and the last maximum is observed at lower magnetic fields than expected from the linear dependence (solid straight line). For a discussion see the text.

magnetic field scale is still maintained when the splitting of both LF oscillations starts to become visible. In the same range the HF oscillation shows a rapid variation of its amplitude while the fundamental frequency changes monotonously according to the anisotropy of the constant-energy surfaces. This is shown in Fig. 8 where

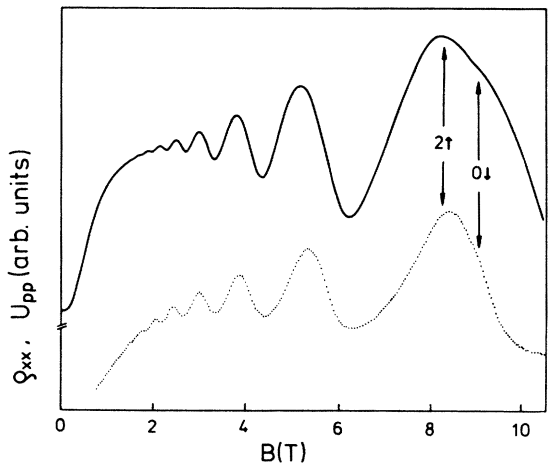

FIG. 7. Experimental results U_{pp} for $\mathbf{B}\|\mathbf{c}$ and $x=0.08$ (solid line) and numerical simulation (ρ_{xx}; dotted line) with $M=1.9$ and $T_D=\Gamma/(\pi k_B)=10$ K (a discussion is in Sec. III).

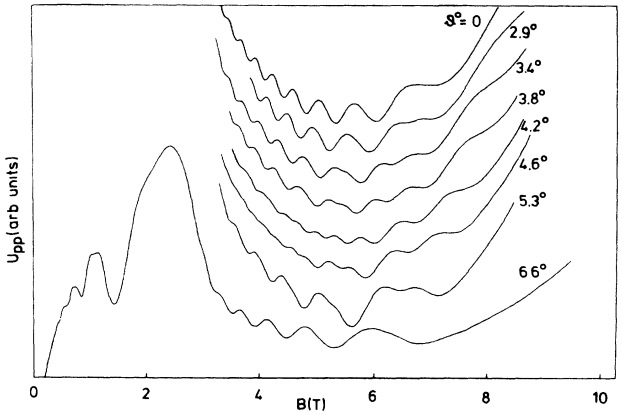

FIG. 8. LF and HF quantum oscillations for $\mathbf{B}\perp\mathbf{c}$ in angular distance $\vartheta=6.6°$ from one of the binary axes ($x=0.09$), and the HF oscillation for various angles $\vartheta<6.6°$.

the tilt angle ϑ is measured from the respective binary axis. A tracing of the different U_{pp} maxima as a function of ϑ reveals the additional splitting of the single maxima (at $\vartheta=0°$ and $|\vartheta|>7°$) for $\vartheta\approx\pm5°$. Twofold differentiation of U_{pp} with respect to B essentially eliminates disturbing background curvature and allows a de-

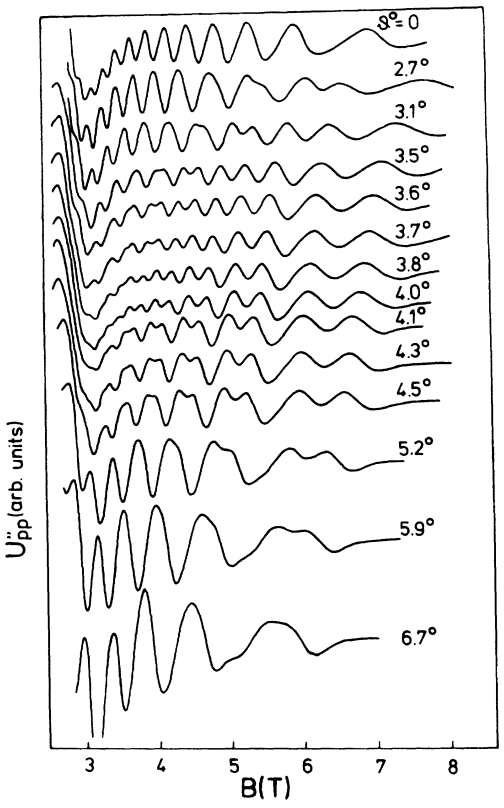

FIG. 9. Second-derivative $U''_{pp}=d^2U_{pp}/dB^2$ for $\mathbf{B}\perp\mathbf{c}$ and various tilt angles with respect to one of the binary axes of a sample with $x=0.09$. The frequency doubling is traversed at $\vartheta=3.5°$–$4°$.

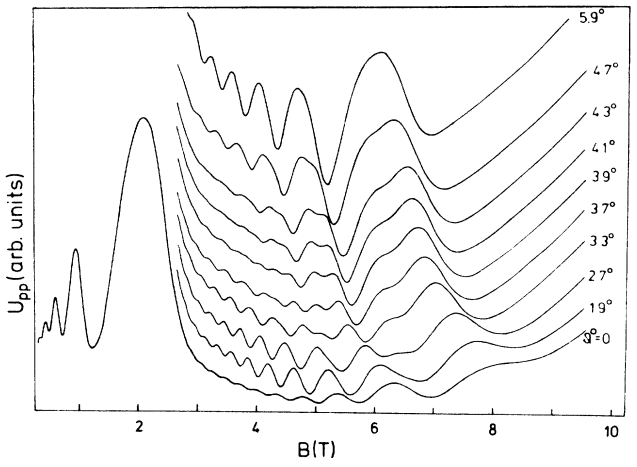

FIG. 10. Magnetoquantum oscillations for a sample with 6% Sb content for $\mathbf{B}\perp\mathbf{c}$. For $\vartheta=0°$ both the LF and HF oscillations are shown; for $\vartheta\neq 0°$ only the HF patterns for $B\gtrsim 2.5$ T are drawn. The intermediate position of the spin-up and -down peaks is reached at about 3.5°.

tailed resolution of additional structure in the HF quantum oscillation where the LF oscillations are already in the quantum limit (Fig. 9). The doubling of the fundamental frequency for $x=0.09$ clearly occurs at almost 4° for $\pm\vartheta$. An energy dependence of $M=\Delta_s/(\hbar\omega_c)$, to be expected for an ENP or more complicated model, by charge transfer between the valleys as a function of B makes the traversing of the half-integer value of M depend on B as demonstrated in Fig. 9.

The principal properties of the magnetoquantum oscillations are maintained when the Sb content is reduced.

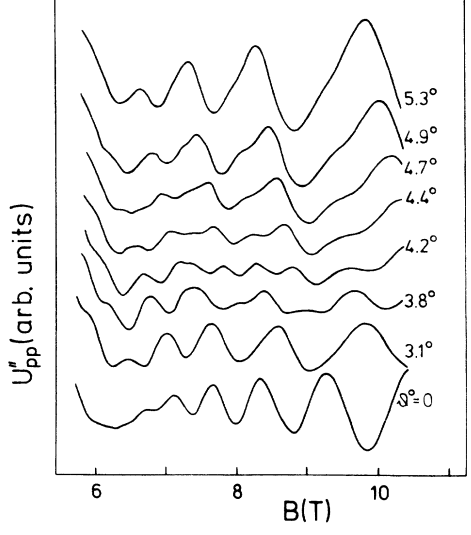

FIG. 11. Second derivative U''_{pp} of the HF oscillation at $\mathbf{B}\perp\mathbf{c}$ and different angles $\vartheta=\sphericalangle(\mathbf{B},\mathbf{n})$ for a crystal with $x=0.02$. Additional structure due to spin splitting is distinctly visible for $\vartheta\approx 4°$.

This is shown in Figs. 10 and 11 for $\mathbf{B}$ almost parallel to one of the binary axes ($\mathbf{B}\perp\mathbf{c}$) and different concentrations, $x=0.06$ and 0.02 as examples. In the latter case, the characteristic features of the HF oscillation are resolved in the second-derivative U''_{pp} only (as a result of a necessary higher doping), in any case revealing the frequency doubling associated with a reduced amplitude for $\mathbf{B}$ some degrees away from the binary axis ($\vartheta=0°$). This maintenance of the basic properties also holds for other orientations in the magnetic field, e.g., for $\mathbf{B}\|\mathbf{c}$, and does not show any marked influence for the L-point zero-gap compositions with $x\approx 0.055$.

Hence, the experimental data directly reveal for arbitrary antimony concentration ($x=0$, 0.02, 0.03, 0.035, 0.04, 0.05, 0.055, 0.06, 0.08, 0.09, 0.10, and 0.12) that M essentially deviates from unity, contrary to the expectation for a two-band model, being half-integer in the vicinity of the maximum cross-sectional area of the Fermi surface and reaching an almost-integer and even value for $\mathbf{B}\|\mathbf{c}$. In particular, the latter is a striking result after almost six decades of research on Bi and Bi-Sb alloys, its revelation becoming possible by a controlled sample preparation concerning the composition and doping. In the following section the numerical simulations of the quantum oscillations are discussed in order to exclude even the smallest possibility for a misinterpretation of the experimental results, which might be induced by electron transfer between the valleys as a function of B.

III. NUMERICAL SIMULATION

The Kubo formalism[15] yields the description of magnetoquantum oscillations in the conductivity (σ_{xx} in the transverse, σ_{zz} in the longitudinal case, and the Hall conductivity σ_{xy}). Our numerical calculations are performed on the reasonable assumption for $T=0$ ($T_{\text{expt}}\approx 1.5$ K). We consider level broadening by scattering (Γ) and use is made of the ENP two-band model for the $E(\mathbf{k})$ relation for the calculation of $E_F(B)$. This should not be quite correct for an essential deviation of $M=\Delta_s/(\hbar\omega_c)$ from unity, however, since the Fermi energy varies appreciably only when the quantum limit is reached, and merely a gross consideration of charge transfer is necessary, we prefer a relation which does not contain too many primarily unknown parameters. The ENP energy dispersion appears to be a reasonable and practicable approximation. The chemical potential (Fermi energy E_F for $T=0$) is calculated first on the efficient approach of a cutoff of the Landau subbands between 5Γ and 10Γ below the respective broadened Landau level ($k_z=0$; $\mathbf{B}\|\mathbf{e}_z$) of Lorentzian shape, i.e., $E_{u\pm}=(n+\frac{1}{2}\pm M/2)\hbar\omega_c-\alpha\Gamma$, with $\alpha=5$–10 (Ref. 12) where the error in E_F(calc) is less than 1%. Hence, the electron concentration N_k within a single valley ($k=1,2,3$) becomes

$$N_k=\frac{eB(m_{zz})^{1/2}}{2\pi^2\hbar^2}(\hbar\omega_c)^{1/2}\times\sum_{n,\pm}\{[x_{F\pm}+(x_{F\pm}^2+\gamma^{*2})^{1/2}]^{1/2}-[x_{u\pm}+(x_{u\pm}^2+\gamma^{*2})^{1/2}]^{1/2}\}\ , \tag{1}$$

with $\gamma^*=\Gamma/[\hbar eB/m_c(0)]$, $x_{i\pm}=E_i(1+E_i/E_g)m_c(0)/(\hbar eB)-(n+\frac{1}{2}\pm M/2)$, and $i=u,F$. In Eq. (1) the ENP energy dispersion is considered and $m_c(0)$ is the band-edge cyclotron mass in the ENP model. The cyclotron mass $m_c(E_F)$ at E_F may be determined from the temperature dependence of the oscillatory amplitude of the quantum oscillations. In the case of significant electron-phonon coupling, however, by emission and reabsorption of virtual phonons, considerable renormalization effects may influence the masses evaluated by this method. In the EP model $m_c^{\rm EP}(E_F)$ is related to $m_c(0)$ (E_g denotes the energy gap):

$$m_c^{\rm EP}(E_F)=m_c(0)(1+2E_F/E_g)\ . \tag{2}$$

m_{zz} is adjusted to yield $\frac{1}{3}$ of $-(eR_{H\infty})^{-1}$ outside the quantum limit [possible neglect of small oscillatory behavior of $E_F(B)$ as a result of level broadening]. In the quantum limit, even of only part of the valleys, electron transfer is considered by numerical adjustment of $E_F=E_{Fk}$ $(k=1,2,3)$.

For $\mathbf{B}\|\mathbf{c}$ a perfect perpendicular alignment of $\mathbf{B}$ and $\mathbf{j}$ ($\mathbf{j}$ denotes the current density) could be managed, but for $\mathbf{B}\perp\mathbf{c}$ ($\mathbf{B}\|\mathbf{s}$ and $\mathbf{B}$ are almost parallel to $\mathbf{n}$) only an approximate transverse configuration could be realized on the same sample. Nevertheless, the error introduced by use of σ_{xx} for the numerical simulations should be negligibly small. Way, Kao, and Wang[16] consider the ENP energy dispersion in σ_{xx}. Their result for finite level broadening and $T=0$ is

$$\sigma_{xx}=\frac{e^2Wm_c(0)m_{zz}(0)}{2(2\pi)^3\hbar^5}(1+2E_F/E_g)^2 \times\sum_{n,\pm}\sum_{n',\pm}\left[(n+n'+1)\hbar\Omega_c\prod_{i=n,n'}\left[\frac{\varepsilon-\left[i+\frac{1}{2}\pm\frac{M}{2}\right]\hbar\Omega_c-\Delta+\left\{\left[\varepsilon-\left[i+\frac{1}{2}\pm\frac{M}{2}\right]\hbar\Omega_c-\Delta\right]^2+\Gamma^2\right\}^{1/2}}{\left[\varepsilon-\left[i+\frac{1}{2}\pm\frac{M}{2}\right]\hbar\Omega_c-\Delta\right]^2+\Gamma^2}\right]^{1/2}\right] \tag{3}$$

with Γ proportional to $B^{2/3}(1+2E_F/E_g)^{4/3}$ as a parameter, where $\Delta=-\Gamma/\sqrt{3}$, $W=$const, $\varepsilon=E_F(1+E_F/E_g)$, and $\Omega_c=eB/m_c(0)$ holds. Equation (3) only contains scattering for maintenance of the spin orientation, which should dominate even for finite spin-orbit coupling. Finally, the energy gaps between the L-band extrema as a function of the antimony content x are calculated according to Golin:[17]

$$E_g=(15.3-270x)\ \text{meV} \tag{4}$$

with $0.02\le x\le 0.12$ for our $Bi_{1-x}Sb_x$ samples.

For $\mathbf{B}\|\mathbf{s}$, the experimental results are easily simulated for $M(\text{LF})=M(\text{HF})\approx 1$ with band-edge masses $m_c(0)_{\rm HF}\approx 2m_c(0)_{\rm LF}$. In this case no essential charge transfer and field dependence of $E_F(B)$ occurs outside the quantum limit (i.e., up to the last oscillatory maximum) and, therefore, in the main the same results are obtained by use of Eq. (3) or a simplified description of σ_{xx} without consideration of nonparabolicity. This applies also to results for $\mathbf{B}\|\mathbf{c}$ outside the quantum limit where, according to Fig. 3, a value of $M\approx 0$ or 2 (instead of 1 in the two-band model) has to be assumed. The numerical calculation in Fig. 3 was performed with $M=0$ and $m_c(0)=(6.2\times 10^{-3})m_0$. The agreement with the experiment (position of the extrema) is perfect.

For $M=0$ all Landau levels are twofold degenerate $(n;\uparrow\downarrow)$, which also applies for $M=1$ $(n\downarrow;n+1\uparrow$, except the lowest level $n=0\uparrow)$ and for $M=2(n\downarrow;n+2\uparrow$, except both lowest levels $n=0\uparrow$ and $n=1\uparrow)$. Therefore, in the last maximum ($B_0\approx 9.5$ T in Fig. 5), which only appears for a finite spin splitting, $E_F(B)$ roughly coincides with the $n=0\downarrow$ level ($M\approx 0$) or the $n=1\uparrow$ level (for $M\approx 2$). The distance from the lowest level is Δ_s ($M\approx 0$) and $\hbar\omega_c$ ($M\approx 2$), respectively. Consequently, a higher electron concentration is contained in the lowest Landau subband $n=0,\uparrow,k_z$ up to $E_F(B_0)$ for $M=2$ in comparison with $M\approx 0$. From this reason, for $M=2$ the last maximum (B_0) is reached at lower fields than for $M\approx 0$ [and $E_F(B_0)\approx(\frac{3}{2}-M/2)\hbar\omega_c=\frac{1}{2}\hbar\omega_c$ becomes field dependent], which causes the deviation from a linear dependence in Fig. 6. Therefore, a numerical simulation is successful only for $M=2$ (or $M\approx 2$)—as for Bi_2Se_3 (Ref. 12)—which is also shown in Fig. 5 [$m_c(0)=0.025m_0$], together with the variation of $E_F(B)$. In the quantum limit $E_F(B)$ for $M=2$ sinks below the conduction-band edge for $B=0$ towards the Landau level $n=0\uparrow$. Within the error margins the agreement with experiment is perfect. For higher electron concentrations a somewhat lower value of about 1.8 might apply in Fig. 7 (causing a slight splitting of the maximum at about 8.5 T), when in the original $U_{\rm pp}$ curve the asymmetry in the maximum is considered. Contributions both from the $2\uparrow$ and $0\downarrow$ levels are weighted by the factor $(n+n'+1)$ in Eq. (3), and this becomes clearly visible even for the same scattering probability. At $B\approx 9$ T the $0\downarrow$ structure is just starting to be resolved for the parameters M and Γ assumed.

In the case of pure bismuth ($x=0$) the amount of doping by Te has to be increased considerably in order to obtain crystals with exclusive n-type conduction. Simultaneously, the mobility of the charge carriers is reduced, rendering the observation of the magnetoquantum oscillations more difficult. On the other hand, for $\mathbf{B}\|\mathbf{c}$ the relative spin splitting M is almost half-integer for undoped bismuth,[18] so that doping, for $M=M(E)$, might improve

the observability of Shubnikov–de Haas oscillations. Actually, for highly doped samples with $(-eR_{H\infty})^{-1} = 3.8\times10^{18}$ cm^{-3} we observed magnetoquantum oscillations for $\mathbf{B}\|\mathbf{c}$ without resolution of spin-splitting structure. The phase of the extrema is compatible with $M\approx2$ as deduced above for $Bi_{1-x}Sb_x$ alloys with $x\geq0.08$, and also corroborated for 6%, 4%, 3.5%, and 2% Sb.

For $\mathbf{B}\perp\mathbf{c}$ and $\vartheta=\sphericalangle(\mathbf{B},\mathbf{n})\approx\pm3°-5°$ a half-integer value of M is traversed (Figs. 8–11) in the HF oscillation. In principle, $\frac{1}{2}$, $\frac{3}{2}$, and even higher half-integers are possible while the first two given are most probable. In order to decide between both cases, for $M(\mathrm{HF})=2$ (approximate value outside the angular range of doubled frequency in the HF Shubnikov–de Haas oscillations) we attempt to simulate the experimental curves by use of Eq. (3), where a finite, but small LF splitting for $\vartheta\neq0°$ is not considered for simplification (the influence on the HF oscillation is unimportant).

It is evident that the consideration of electron transfer between the valley systems and of nonparabolicity [Eq. (3)] becomes absolutely necessary for an optimized fitting. Exclusively in this case, the principal field dependence of the oscillatory amplitudes may be attained. For $M(\mathrm{HF})\approx2$, instead of $M(\mathrm{HF})\approx0$, the last U_{pp} maximum is reached at essentially lower magnetic fields (see the discussion above for $\mathbf{B}\|\mathbf{c}$). The numerical simulation in Fig. 12 for $M(\mathrm{HF})=2M(\mathrm{LF})=2$ and $m_c(0)_{\mathrm{HF}} = (5.5\times10^{-3})m_0$ shows that an agreement with the experimental data at $\vartheta=7°$ may be achieved (except for the splitting of the LF oscillation not considered in the calculation) where an extremely weak $n=1\uparrow$ maximum is reached at $B\approx10$ T in the calculation. Since a realization of this structure in the experiment cannot be attained for $B_{\max}=10$ T, lower electron concentrations are necessary in order to decide if $M(\mathrm{HF})\approx2$ is reached and where this occurs (at $\vartheta\approx0°$ or 7°). In Fig. 12 the numerical data are completed by the variation of $E_F(B)$, essentially resulting in an electron transfer between the valleys for $B\gtrsim2.5$ T, where the quantum limit of the LF systems begins, accompanied by a reduction of the electron concentration in the HF system (see the discussion in connection with Fig. 2).

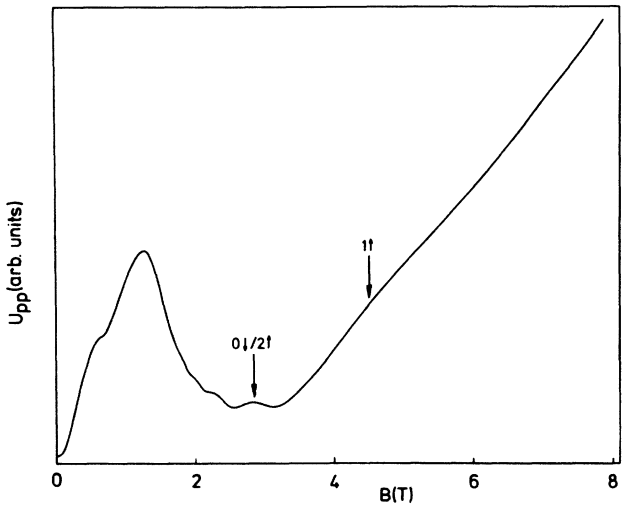

FIG. 13. Experimental magnetoquantum oscillations for $\mathbf{B}\perp\mathbf{c}$ and $\vartheta=7°$ of a sample with $x=0.1$ and low electron concentration. The arrows identify the $n=1\uparrow$ and $n=2\uparrow/0\downarrow$ maxima in the HF oscillation, corresponding to a realization of a relative spin splitting $M\approx2$ as calculated numerically in Fig. 12 for a somewhat higher doping.

Finally, in Fig. 13 for a sample with low electron con-

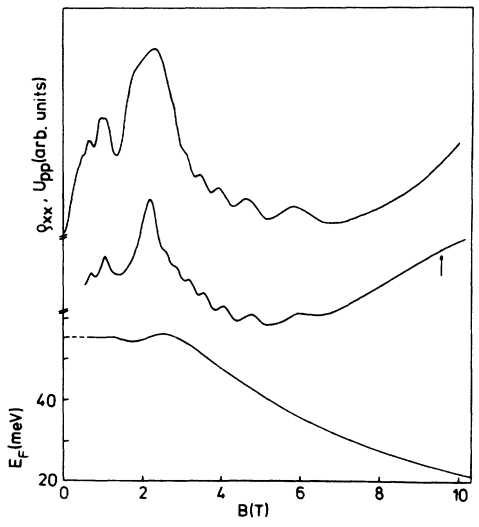

FIG. 12. Experiment (U_{pp}; $x=0.09$) and numerical simulation of ρ_{xx} and E_F with $M(\mathrm{LF})=1$ and $M(\mathrm{HF})=2$ for $\mathbf{B}\perp\mathbf{c}$ and $\vartheta=7°$. The arrow at about 10 T in the numerical simulation indicates the approximate position where the $n=1\uparrow$ maximum should be expected. A discussion is in the text.

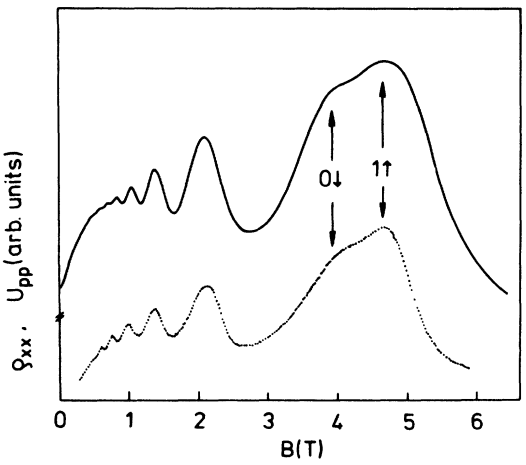

FIG. 14. Experimental results for U_{pp} (solid curve) obtained with $\mathbf{B}\|\mathbf{n}$ for the low-frequency oscillation (LF) on a sample with $x=0.02$. The indication of spin splitting near $B=4$ T is simulated numerically (dotted curve) with $M=1.15$ and $T_D=20$ K.

centration and $x=0.1$ the $n=1\uparrow$ maximum ($\mathbf{B}\perp\mathbf{c}$ and $\vartheta=7°$) is reached at $B\approx4.5$ T (arrow), which may be simulated numerically with $M(\mathrm{HF})=2$. The occurrence of this maximum excludes a description by $M(\mathrm{HF})\approx M(\mathrm{LF})\approx1$ since, in this case, $E_F(B)$ in the quantum limit approaches the coinciding $0\uparrow$ LF and HF levels in the band edge. For $M(\mathrm{HF})\approx0$, e.g., in Fig. 8 ($x=0.09$) the relative weighting of the peaks by the Landau quantum numbers n and n' [Eq. (3)] within the camelback structures at, for instance, $\vartheta=5.3°$ should be the same with respect to the upper envelope,[19] which does not apply. Consequently, for $\vartheta_0=3°-5°$ the ratio $M=\Delta_s/(\hbar\omega_c)=\frac{3}{2}$ is traversed for the HF oscillation and $M(\mathrm{HF})<\frac{3}{2}$ applies for $0\le\vartheta<\vartheta_0$ and $M(\mathrm{HF})>\frac{3}{2}$ for $\vartheta>\vartheta_0$.

In Fig. 14, for $x=0.02$, spin-splitting structure is resolved in the LF magnetoquantum oscillation for $\mathbf{B}\|\mathbf{n}$ near 4–5 T, which is simulated with $M=1.15$ and $T_D=\Gamma/(\pi k_B)=20$ K, indicating that M again has dropped below $\frac{3}{2}$ at $\vartheta=\pm60°$ ($\mathbf{B}\perp\mathbf{c}$).

IV. COMPARISON WITH PURE BISMUTH

Our experimental results on $Bi_{1-x}Sb_x$ single crystals with a particular, single-charge carrier preparation for arbitrary composition ($0\le x\le0.12$) show a considerable anisotropy of the relative spin splitting $M=\Delta_s/(\hbar\omega_c)=gm_c/(2m_0)$ (as deduced also for Bi_2Te_3[13,14]), which is in clear contradiction to the two-band model assumed for many purposes. The data of the L conduction electrons confirm that the $M=\frac{3}{2}$ transition of the HF oscillation for $\mathbf{B}\perp\mathbf{c}$ and a few degrees from one of the binary axes is maintained down to the lowest antimony concentrations ($x=0.02$). Equivalently, for $\mathbf{B}\|\mathbf{c}$ (including $x=0$) the ratio of the spin and cyclotron splitting M for our doped samples shows values near 2 in the whole range of compositions.

A comparison with the results of Takano and Koga[18] is close at hand, where spin-splitting factors (γ) were deduced for electrons in pure and undoped bismuth. Quantum oscillations in the velocity of sound were investigated for $\mathbf{B}$ within the trigonal, binary, and bisectrix planes. In the latter case results for $\mathbf{B}$ near the trigonal axis are sparse in the range of the strongest variation of γ for this configuration, and outside it roughly constant values $\gamma\approx1.1$ are deduced starting from $\mathbf{B}\|\mathbf{n}$, which is also obtained from our experiments in a wide angular range ($\gamma\approx M$).

The angular spectra, where spin splitting may be observed and assigned reliably, are separated by gaps where no structure from spin splitting may be evaluated. Since Takano and Koga[18] do not perform phase analyses for their magnetoquantum oscillations and since they do not reach the quantum limit in their experiments, a correction of their values deduced for γ might become necessary, because only the effective spin splitting is observed primarily. A reliable determination of the absolute value for $M=\gamma,\ 1\pm\gamma,\ 2\pm\gamma,\ \ldots$ mostly needs further information. This holds more when only restricted sections of the angular spectrum are accessible to a reliable evaluation.

Though the absolute values of M may differ somewhat between our and the Takano and Koga experiments, resulting from different composition (x) and doping (Te), the characteristic ranges for M should be the same. We have reliable information (see the discussion above) that M should be higher than $\frac{3}{2}$ for $\mathbf{B}\|\mathbf{c}$ ($M\approx2$ in our case) and be higher than $\frac{3}{2}$ for $\mathbf{B}\perp\mathbf{c}$ and $|\vartheta|=|\sphericalangle(\mathbf{B},\mathbf{n})|\gtrsim4°$. In Figs. 15 and 16 we show the evaluation of Takano and Koga[18] and our modification of their data (γ) by $M=1+\gamma$ for $\mathbf{B}\perp\mathbf{c}$ and small $|\vartheta|\lesssim10°$ (Fig. 15; $\mathbf{B}$ in the trigonal plane) and by $M=2-\gamma$ for $\mathbf{B}\|\mathbf{c}$ and its nearest vicinity (Fig. 16; $\mathbf{B}$ in the binary plane). We propose these as the most convenient and most probable interpretations for M, in agreement with our results discussed above.

It is obvious that, in our interpretation, $M\sim gm_c$ reaches sharp maxima only a few degrees away from the maximum extremal cross-sectional areas of the L Fermi surfaces, i.e., for k_y almost parallel to the respective k plane normal to $\mathbf{B}$. This holds for $\mathbf{B}$ in the trigonal (Fig. 15) and in the binary plane (Fig. 16). Usually the anisotropy of the effective mass (m_c) is cancelled by the opposite of the effective g factor, which does not apply here. However, a similar anisotropy, differing in magnitude for

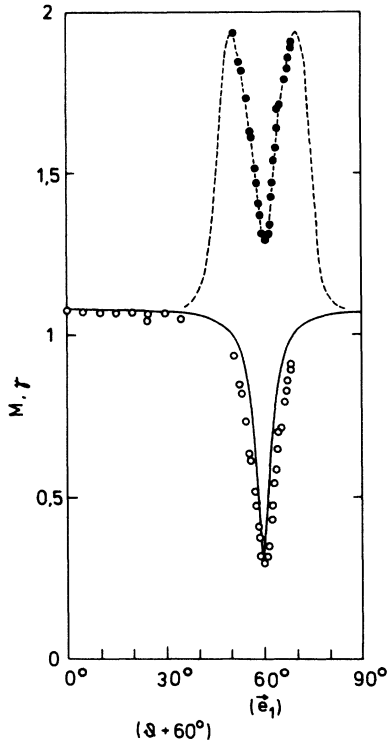

FIG. 15. Spin-splitting factors of Takano and Koga (Ref. 18) (γ; open circles and solid line) with $\mathbf{B}$ in the trigonal plane for pure bismuth ($x=0$), and our interpretation $M=1+\gamma$ (solid circles and dashed line) for $50°\le\vartheta+60°\le70°$ and $M=\gamma$ outside this range. $\vartheta=0°$ corresponds to the maximum of the extremal cross-sectional area of the respective Fermi surface.

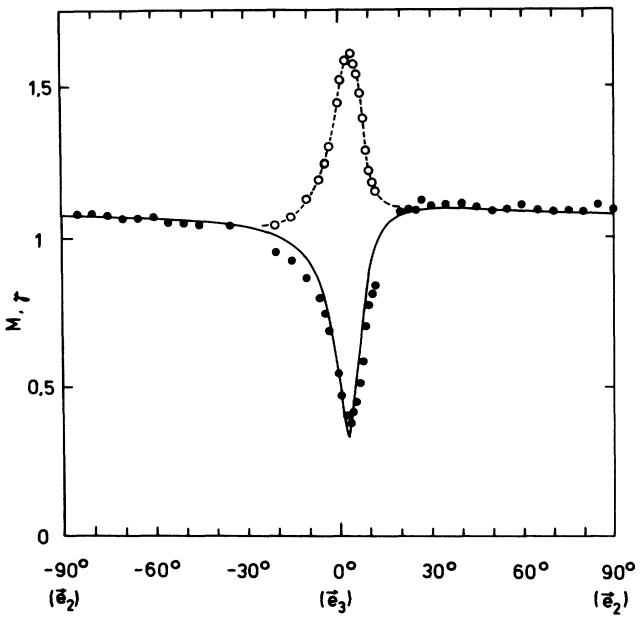

FIG. 16. Spin-splitting factors γ of Takano and Koga (Ref. 18) for Bi (solid circles and solid line) with **B** in the binary plane, and our interpretation $M=2-\gamma$ (open circles and dashed line) in the angular range between $-20°$ and $10°$ and $M=\gamma$ outside it.

m_c and g, may be assumed tentatively and, hence, the $E(\mathbf{k})$ relation separately allows a discussion of the anisotropy of $M \sim g m_c$.

McClure and Choi[4] have proposed a modified NENP model (MNENP) which includes third-order $\mathbf{k}\cdot\mathbf{p}$ terms with the greatest importance, such as $k_y^3 k_z$, k_y^4, $k_y^2 k_z^2$, and $k_y^2 k_x^2$. McClure and Choi conclude that the first two should be of minor importance, while Chen *et al.*[20] propose an additional influence of the k_y^4 term and neglect the effect of the $k_y^3 k_z$ only. They rewrite the dispersion relation as

$$E\left[1+\frac{E}{E_g}\right]=\frac{\hbar^2 k_x^2}{2m_x}+\frac{\hbar^2 k_y^2}{2m_y}\left[1+\frac{E}{E_g}\left[1-\frac{m_y}{m_y'}\right]\right]+\frac{\hbar^2 k_z^2}{2m_z}+\frac{\hbar^4 k_y^4}{4m_y m_y' E_g}-\frac{\hbar^4 k_x^2 k_y^2}{4m_x m_y E_g}-\frac{\hbar^4 k_y^2 k_z^2}{4m_y m_z E_g}\,. \tag{5}$$

In a reasonable approximation $m_y \approx m_y'$ is usually assumed.

Deviations of M from unity, therefore, have to result from the k^4 terms in Eq. (5). In Figs. 15 and 16, in our interpretation, maximum effects occur for finite k_x values, i.e., for $\mathbf{B}\|\mathbf{e}_z$ (Fig. 16) and for $\mathbf{B}\perp\mathbf{c}$ with $|\vartheta|\approx 10°$ (Fig. 15). This means that the influence of the term $-\hbar^4 k_x^2 k_y^2/(4m_x m_y E_g)$ in Eq. (5) should be of essential importance, showing large anisotropy with a maximum for **B** near the binary axis, e.g., for $\mathbf{B}\perp\mathbf{c}$. According to the magnitude of the main mass parameters, the term proportional to $k_y^2 k_z^2$ should contain a less dramatic variation with the angle $\sphericalangle(\mathbf{B},\mathbf{e}_z)=90°-\sphericalangle(\mathbf{e}_y,\mathbf{B})$, and, therefore, upon increasing $|\vartheta|$ (for $\mathbf{B}\perp\mathbf{c}$) the variation of the next-to-last term in Eq. (5) primarily dominates over variation of the last term. Vice versa, for **B** in the binary plane (in the vicinity of $\mathbf{B}\|\mathbf{e}_z$) this effect does not occur, corresponding to a smoother curvature of $M=g m_c/(2m_0)$ in Fig. 16. Consequently, the mixed k^4 terms in Eq. (5) are indispensible for a comprehensive interpretation of the angular dependence of the spin-splitting ratio M in Bi and $Bi_{1-x}Sb_x$ alloys.

According to Golin[17] for bismuth ($x=0$) the electrons of concern in the conduction band with a minimum at L are in a symmetric $L_s=L_5+L_6$ state (0.282 40 a.u.) and should interact with several antisymmetric $L_a=L_7+L_8$ states nearby, e.g., with the valence band with a maximum at 0.281 83 a.u. and the more distant states at 0.215 27, 0.338 67 a.u., etc. Therefore, at least a four-band model, including spin-orbit coupling, should be necessary, leading to an energy dispersion of the type of Eq. (5), which also enters into the Landé g tensor and cyclotron-mass tensor. The point is whether the parameters of both the last terms (and of the fourth) on the right side of Eq. (5) have to be assumed to be that large, as was done by Chen *et al.*[20] and Cankurtaran *et al.*,[21] in order to avoid the effects discussed in the latter paper, that closed orbits should no longer possibly occur for particular orientations in the magnetic field. So far, there seem to be no indications for such an effect, which certainly should show up in a dramatic manner where $E_g=0$ is reached for $x\approx 0.055$. On both sides of this alloy concentration no significant changes in the spin-splitting characteristics [$M=g m_c/(2m_0)$] are observed at finite Fermi energies above the minimum of the respective conduction band. This makes it uncertain if the energy gap E_g in the denominators of the last three terms on the right side of Eq. (5) should be that between *the* L-point conduction [0.282 40 a.u. (Ref. 17) and *the* valence band [0.281 83 a.u. (Ref. 17)] and, hence, if the interaction with the more distant bands should not be predominantly responsible for the mixed k^4 terms.

V. CONCLUSION

The experimental data obtained in this paper concern homogeneous single crystals of $Bi_{1-x}Sb_x$ alloys with exclusive electron conduction (doping by Te) down to lowest Sb concentrations x. In contrast to pure undoped bismuth ($x=0$) only a single type of charge carrier contributes at low temperatures, therefore implying a higher reliability for the evaluation until the quantum limit is achieved here. Doping has to be increased with decreasing x in order to maintain exclusive conduction by electrons.

Nevertheless, the extreme anisotropy of the $E(\mathbf{k})$ relation and the existence of three equivalent L-point constant-energy surfaces complicate a general investigation. Only for the main symmetry axes is the number of different extremal cross-sectional areas of the Fermi sur-

faces reduced to 1 ($\mathbf{B}\|\mathbf{c}$) and 2 ($\mathbf{B}\|\mathbf{s}$ and $\mathbf{B}\|\mathbf{n}$), allowing a more detailed examination. Even for $\mathbf{B}\|\mathbf{s}$ the superposition of both Shubnikov–de Haas oscillations is perfect (frequency ratio of about 2:1), and the analysis of the spin splitting is compatible with $M(\mathrm{HF})\approx M(\mathrm{LF})\approx 1$, in reasonable agreement with the two-band model. The results for $\mathbf{B}\|\mathbf{c}$ exclude a value of $M\approx 1$ and may be explained by theory with $M\approx 2$ exclusively. For $\mathbf{B}\perp\mathbf{c}$ and $\mathbf{B}\|\mathbf{n}$ the ratio of the spin and cyclotron splitting also approaches unity (largest extremal cross-sectional area), but rapidly increases above $\frac{3}{2}$ some degrees off from $\mathbf{B}\|\mathbf{n}$ perpendicular to the $\mathbf{c}$ axis, approaching $M\approx 2$ within a few degrees, equivalent to $\mathbf{B}\|\mathbf{c}$. An experimental connection of both results at intermediate tilt angles of our doped and alloyed samples cannot be realized so far owing to the problems discussed.

Our experimental results for $x\rightarrow 0$ allow a comparison with pure bismuth. They confirm that also for $x=0$ the spin splitting essentially increases above the cyclotron energy for some orientations of $\mathbf{B}$ discussed above. Hence, a reinterpretation of the spin-splitting factors deduced by Takano and Koga[18] from the high-resolution data of Bi samples outside the magnetic quantum limit permits a connection to the energy-band model derived by McClure and Choi,[4] including $\mathbf{k}\cdot\mathbf{p}$ terms up to the third order. On this basis a comprehensive interpretation becomes possible exclusively when the $k_x^2k_y^2$ and $k_y^2k_z^2$ contributions in the $E(1+E/E_g)$ dispersion are considered.

[1] L. Shubnikov and W. J. de Haas, Leiden Commun. **207a**, **207c**, **207d**, and **210a** (1930).

[2] B. Lax, Phys. Rev. **114**, 90 (1959).

[3] M. H. Cohen, Phys. Rev. **121**, 387 (1961).

[4] J. W. McClure and K. H. Choi, Solid State Commun. **21**, 1015 (1977).

[5] M. H. Cohen and E. I. Blount, Philos. Mag. **5**, 115 (1960).

[6] G. E. Smith, G. A. Baraff, and J. Rowell, Phys. Rev. **135**, A1118 (1964).

[7] B. McCombe and G. Seidel, Phys. Rev. **155**, 633 (1967).

[8] A. A. Abrikosov and L. A. Falkovsky, Zh. Eksp. Teor. Fiz. **43**, 1089 (1962) [Sov. Phys.—JETP **16**, 769 (1963)]; A. A. Abrikosov, Zh. Eksp. Teor. Fiz. **38**, 1031 (1973) [Sov. Phys.—JETP **38**, 1031 (1974)].

[9] G. A. Baraff, Phys. Rev. **137**, A842 (1965).

[10] M. Maltz and M. S. Dresselhaus, Phys. Rev. B **2**, 2877 (1970); M. P. Vecchi and M. S. Dresselhaus, *ibid.* **9**, 3257 (1974); **10**, 771 (1974).

[11] M. S. Dresselhaus, J. Phys. Chem. Solids **32**, Suppl. 1, 3 (1971).

[12] H. Köhler and E. Wüchner, Phys. Status Solidi B **67**, 665 (1975).

[13] H. Köhler, Phys. Status Solidi B **75**, 127 (1976).

[14] H. Köhler, Phys. Status Solidi B **75**, 441 (1976).

[15] R. Kubo, S. J. Miyake, and N. Hashitsume, in *Solid State Physics*, edited by F. Seitz and D. Turnbull (Academic, New York, 1965), Vol. 17, p. 269.

[16] Y.-S. Way, Y.-H. Kao, and S.-y. Wang, Phys. Rev. B **8**, 3500 (1973).

[17] S. Golin, Phys. Rev. **166**, 643 (1968).

[18] S. Takano and M. Koga, J. Phys. Soc. Jpn. **42**, 853 (1977).

[19] H. Köhler and A. Freudenberger, Phys. Status Solidi B **84**, 195 (1977).

[20] M. H. Chen, C. C. Wu, and C. J. Lin, J. Low Temp. Phys. **55**, 127 (1984).

[21] M. Cankurtaran, M. Önder, H. Celik, and T. Alper, J. Phys. C **20**, 3875 (1987).